Supplementary information

Blood–Brain Barrier-Penetrant Nanotherapy Inhibits Haem Oxygenase-1-Mediated Ferroptosis for Post-Resuscitation Neuroprotection

Mao Zhang[1,2,3,#], Wenbin Zhang[1,2,3,#], Qiuyu Wei[4,5,6#], Lu He[1,2,3], Jinyu Zhu[1,2,3], Jiaying Chen[4,5,6], Jiajia Xiang[1,4,5,6*], Youqing Shen[4,5,6*], Jiefeng Xu[1,2,3,*]

[1] Department of Emergency Medicine, Second Affiliated Hospital of Zhejiang University School of Medicine, Hangzhou, China.

[2] Zhejiang Key Laboratory of Trauma, Burn, and Medical Rescue, Hangzhou, China.

[3] Zhejiang Province Clinical Research Center for Emergency and Critical Care Medicine, Hangzhou, China.

[4] Zhejiang Key Laboratory of Smart Biomaterials, College of Chemical and Biological Engineering of Zhejiang University, Hangzhou, China.

[5] Center for Bionanoengineering, College of Chemical and Biological Engineering of Zhejiang University, Hangzhou, China.

[6] Key Laboratory of Biomass Chemical Engineering of the Ministry of Education, College of Chemical and Biological Engineering, Zhejiang University, Hangzhou, China.

[#] These authors contributed equally: Mao Zhang, Wenbin Zhang, Qiuyu Wei

*Correspondence to xiang_jj@zju.edu.cn (J.J.X.), shenyq@zju.edu.cn (Y.S.), z2jeffxu@zju.edu.cn (J.X.)

Supplementary Figures

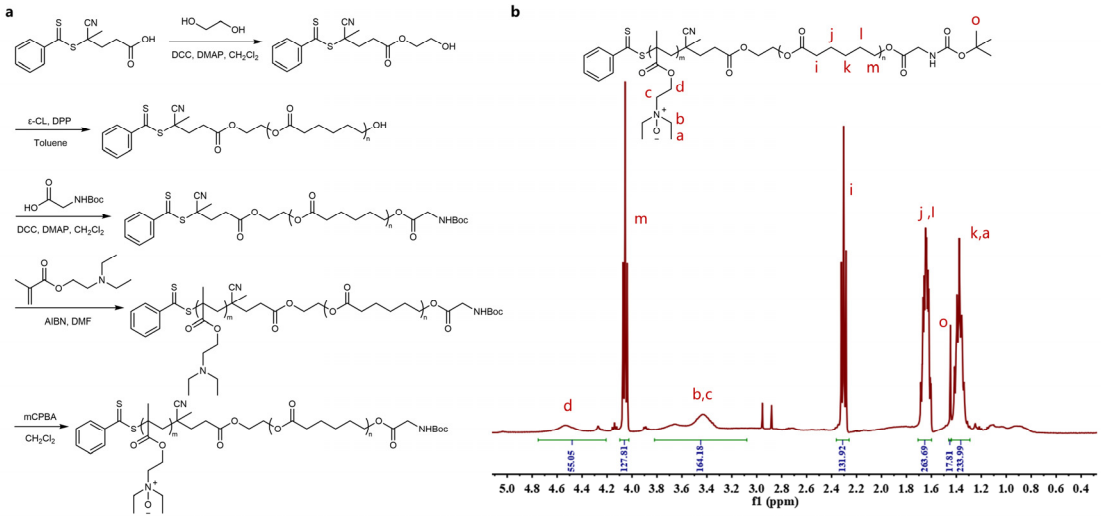

Supplementary Fig. 1 | Synthesis and characterisation of OPDEA-PCL block copolymer. a, The synthetic route to OPDEA-PCL. **b**, The ^{1}H NMR spectrum of OPDEA-PCL in $CDCl_3$.

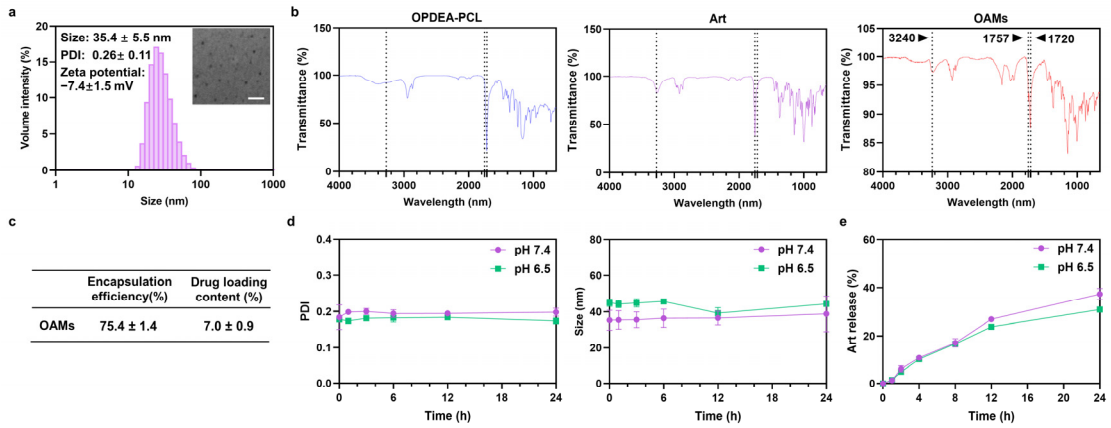

Supplementary Fig. 2 | Physicochemical characterisation of OAMs. a, Hydrodynamic diameter distribution of OAMs measured by dynamic light scattering (DLS); inset, transmission electron microscopy (TEM) image of micelles. Scale bar, 100 nm. The TEM image is representative of $n = 3$ independent replicates. **b**, Fourier-transform infrared (FTIR) spectra of OPDEA–PCL, Art, and OAMs. **c,** Encapsulation efficiency and drug loading content of Art in the micelles measured by high-performance liquid chromatography (HPLC). $n = 3$ independent experiments. **d**, Evaluation of the colloidal stability of OAMs over time in phosphate-buffered saline (PBS) at 37 ℃ by monitoring the hydrodynamic diameter and polydispersity index (PDI) at pH 7.4 or 6.5. **e**, *In vitro* release profiles of Art from OAMs in PBS (37 °C) at pH 7.4 and pH 6.5 over 24 h (initial Art concentration, 200 μg ml^{-1}). Data are shown as mean ± SD ($n = 3$ independent experiments).

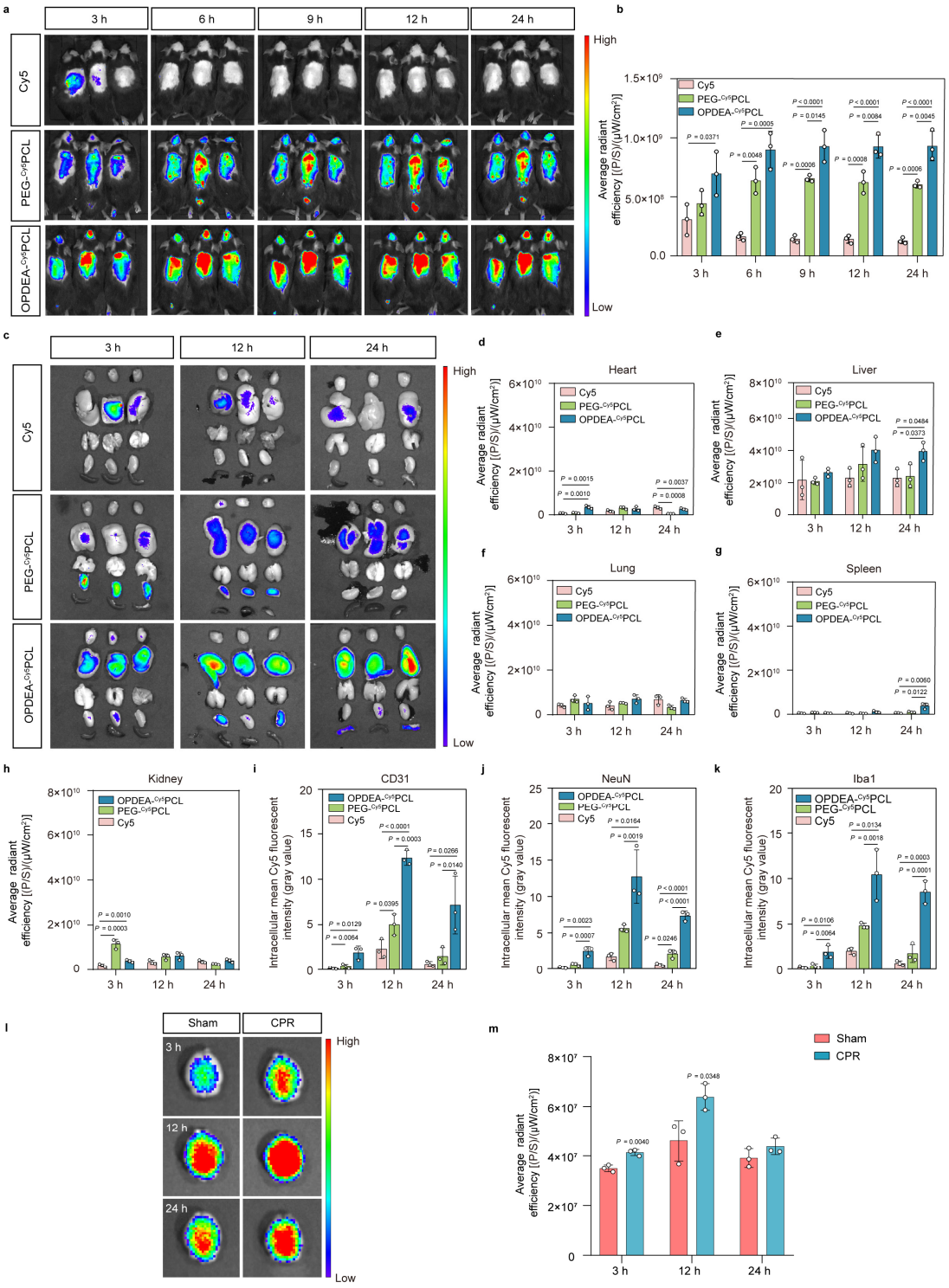

Supplementary Fig. 3 | Biodistribution of OPDEA–PCL micelles in mice. a, b, *In vivo* fluorescence imaging (**a**) and corresponding quantification (**b**) of C57BL/6 mice at designated time points following a single intravenous (*i.v.*) injection of free Cy5, PEG–^{Cy5}PCL, or OPDEA–^{Cy5}PCL micelles. Cy5-equivalent dose, 100 μg kg^{-1}. n = 3 mice. **c–h**, *Ex vivo* fluorescence imaging of major organs (**c**) and quantification of Cy5 signal in the heart (**d**), liver (**e**), lungs (**f**), spleen (**g**), and kidneys (**h**) at the indicated

time points after *i.v.* administration of free Cy5, PEG–^{Cy5}PCL, or OPDEA–^{Cy5}PCL micelles. Cy5-equivalent dose, 100 μg kg^{-1}. n = 3 mice. **i–k**, Quantification of Cy5 fluorescence in CD31^{+} endothelial cells (**i**), NeuN^{+} neurons (**j**), and Iba1^{+} microglia (**k**) at designated time points after *i.v.* administration of free Cy5, PEG–^{Cy5}PCL, or OPDEA–^{Cy5}PCL micelles. Cy5-equivalent dose, 100 μg kg^{-1}. n = 3 mice; 3 randomly selected fields per sample. **l, m**, *Ex vivo* fluorescence imaging (**l**) and quantification (**m**) of brain tissues from Sham and CPR mice at 3, 12, and 24 h post-injection of OPDEA–^{Cy5}PCL micelles. Cy5-equivalent dose, 100 μg kg^{-1}. n = 3 mice. Data are presented as mean ± SD. Statistical significance was determined by a two-tailed unpaired Student's t test (two groups) or one-way ANOVA with Tukey's post hoc test (multiple groups).

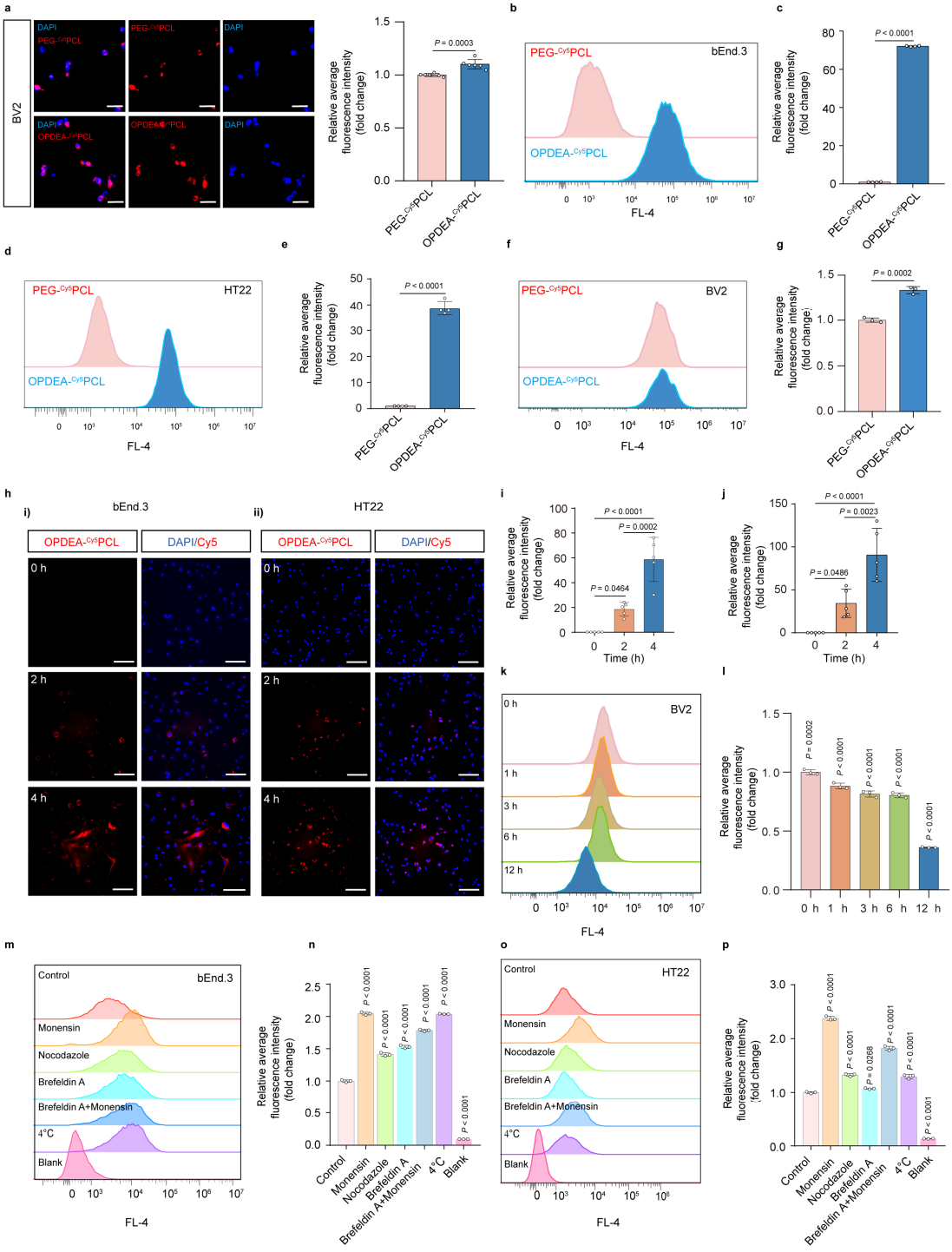

Supplementary Fig. 4 | Cellular uptake, intracellular trafficking, and exocytosis of OPDEA–PCL micelles in endothelial, neuronal, and microglial cells. a, Confocal microscopy images (left) and quantitative analysis (right) of cellular uptake of Cy5-labelled OPDEA–PCL micelles by BV2 microglial cells after 24 h incubation. Nuclei were stained with DAPI (blue). Cy5-equivalent dose, 0.5 μg ml^{-1}. Scale bar, 20 μm. The images are representative of n = 6 biological replicates. **b–g**, Representative flow

cytometry histograms (**b, d, f**) and corresponding quantification (**c, e, g**) of Cy5-labelled micelle uptake in bEnd.3 endothelial cells (**b, c**), HT22 neuronal cells (**d, e**), and BV2 microglial cells (**f, g**) after 24 h incubation (n = 4 biological replicates for panels b, d, and n = 3 for panel f). Cy5-equivalent dose, 0.5 μg ml^{-1}. n = 4 independent experiments for panels c and e; n = 3 independent experiments for panel g. **h**, Time-dependent uptake of OPDEA–^{Cy5}PCL micelles visualised by confocal microscopy in bEnd.3 (**i**) and HT22 (**ii**) cells. Nuclei were stained with Hoechst (blue). Cy5-equivalent dose, 0.5 μg ml^{-1}. Scale bars, 100 μm. The images are representative of n = 5 biological replicates. **i, j**, Quantification of relative Cy5 fluorescence intensity in bEnd.3 (**i**) and HT22 (**j**) cells corresponding to panel **h**. n = 5 biological replicates. **k, l**, Representative flow cytometry histogram (**k**) and quantification (**l**) of time-dependent exocytosis of OPDEA–^{Cy5}PCL micelles from BV2 microglial cells. Cells were pre-incubated with micelles for 24 h, washed, and transferred to fresh medium for the indicated durations. Cy5-equivalent dose, 0.5 μg ml^{-1}. n = 3 independent experiments. **m–p**, Representative histograms (**m, o**) and quantification (**n, p**) of micelle exocytosis pathways in bEnd.3 (**m, n**) and HT22 (**o, p**) cells. Following 24 h incubation with Cy5-labelled micelles, cells were washed and treated for 6 h with inhibitors targeting distinct exocytosis pathways. Cy5-equivalent dose, 0.5 μg ml^{-1}. n = 3 independent experiments. Data are presented as mean ± SD. Statistical significance was determined by a two-tailed unpaired Student's t test (two groups) or one-way ANOVA with Dunnett's multiple comparison test (multiple groups).

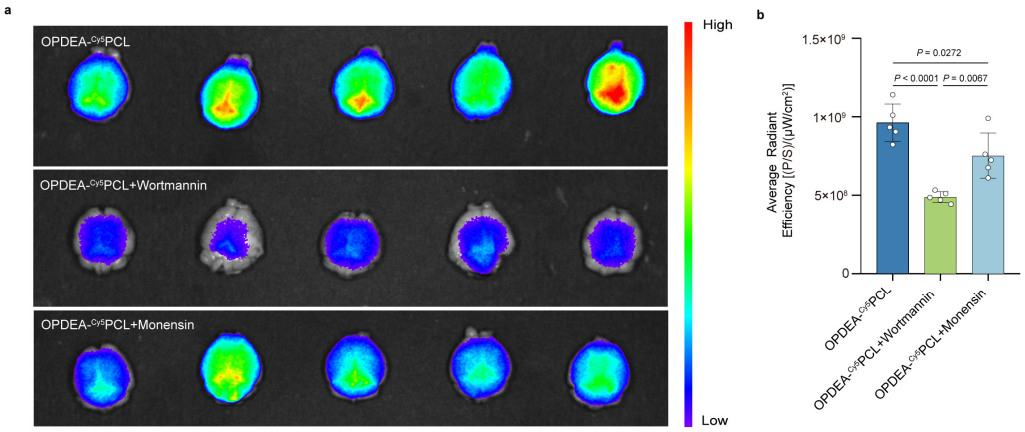

Supplementary Fig. 5 | Brain accumulation of OPDEA–^{Cy5}PCL micelles after pharmacological modulation of endocytosis and exocytosis. *Ex vivo* fluorescence imaging (**a**) and quantitative analysis (**b**) of OPDEA–^{Cy5}PCL micelle accumulation in brain tissues 24 h after *i.v.* injection in mice pretreated with wortmannin (endocytosis inhibitor, 1 mg kg^{-1}) or monensin (exocytosis inhibitor, 10 mg kg^{-1}) for 1 h. n = 5 mice. Data are presented as mean ± SD. Statistical significance was determined by one-way ANOVA with Dunnett's multiple comparison test (multiple groups).

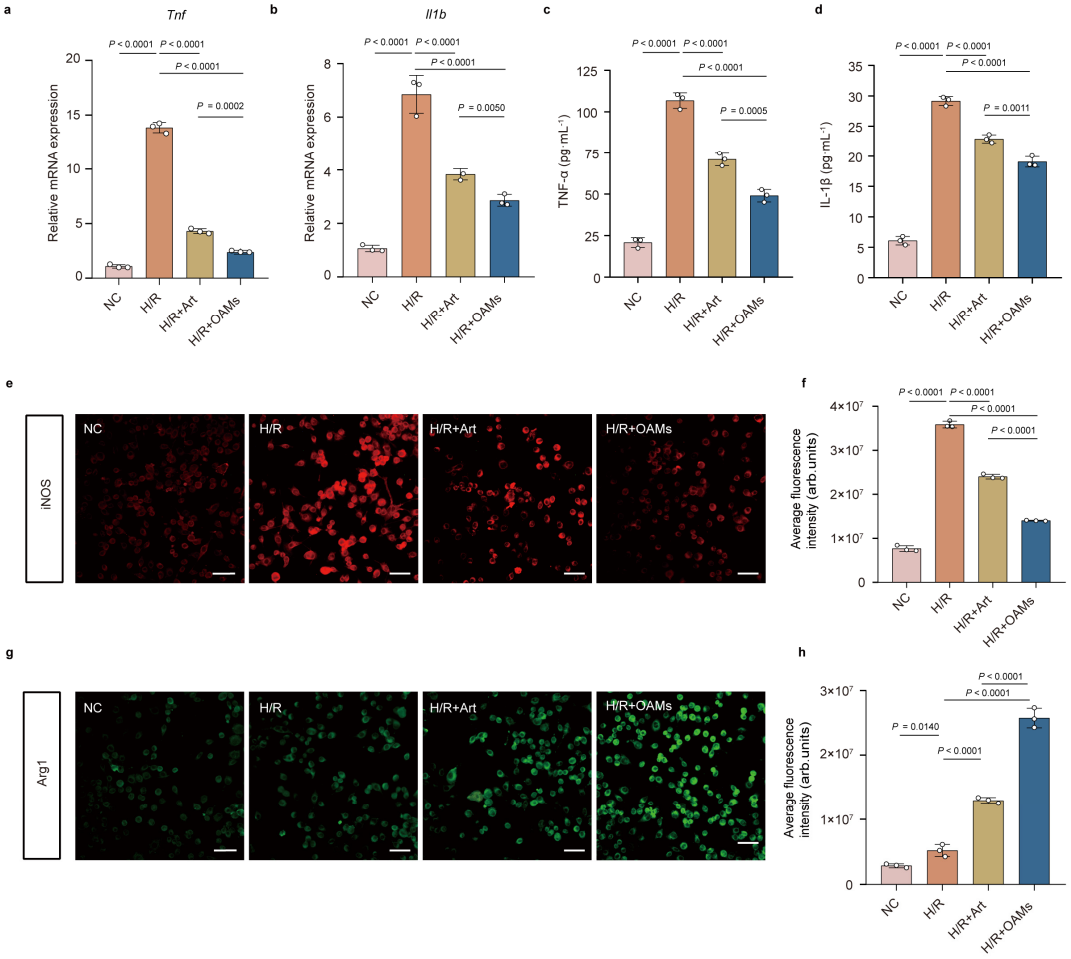

Supplementary Fig. 6 | OAMs attenuate microglial inflammation and reprogramme microglial polarisation. a–d, Relative mRNA expression of *Tnf* (**a**) and *Il1b* (**b**) in BV2 microglial cells treated with OAMs for 24 h under hypoxia–reoxygenation (H/R), as assessed by qRT–PCR; corresponding TNF-α (**c**) and IL-1β (**d**) protein levels in culture supernatants measured by ELISA. Art-equivalent dose, 250 nM. $n = 3$ independent experiments. **e–h**, Immunofluorescence images of BV2 cells stained for the M1 marker iNOS (red) and M2 marker Arg1 (green) after 24 h of H/R with or without OAMs (**e, g**), and quantification of iNOS (**f**) and Arg1 (**h**) fluorescence intensity. Art-equivalent dose, 250 nM. Scale bar, 100 μm. The images are representative of $n = 3$ biological replicates. Data are presented as mean ± SD. Statistical significance was determined by one-way ANOVA with Tukey's post hoc test (multiple groups).

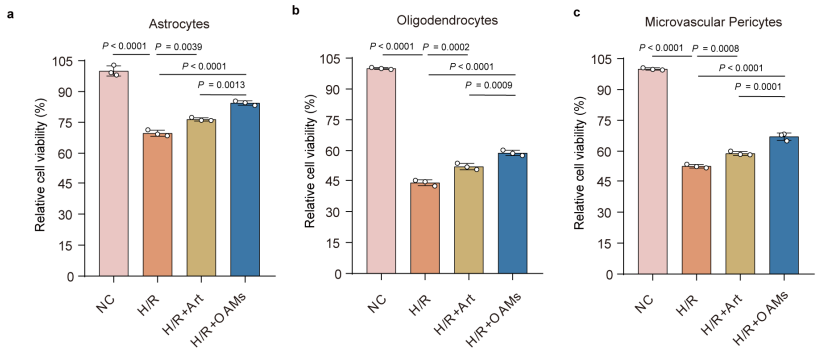

Supplementary Fig. 7 | OAMs preserve viability of multiple neurovascular unit cell types under H/R. Viability of primary astrocytes (**a**), oligodendrocytes (**b**), and brain microvascular pericytes (**c**) treated with OAMs for 24 h under H/R. Art-equivalent dose, 250 nM. n = 3 independent experiments. Data are presented as mean ± SD. Statistical significance was determined by one-way ANOVA with Tukey's post hoc test (multiple groups).

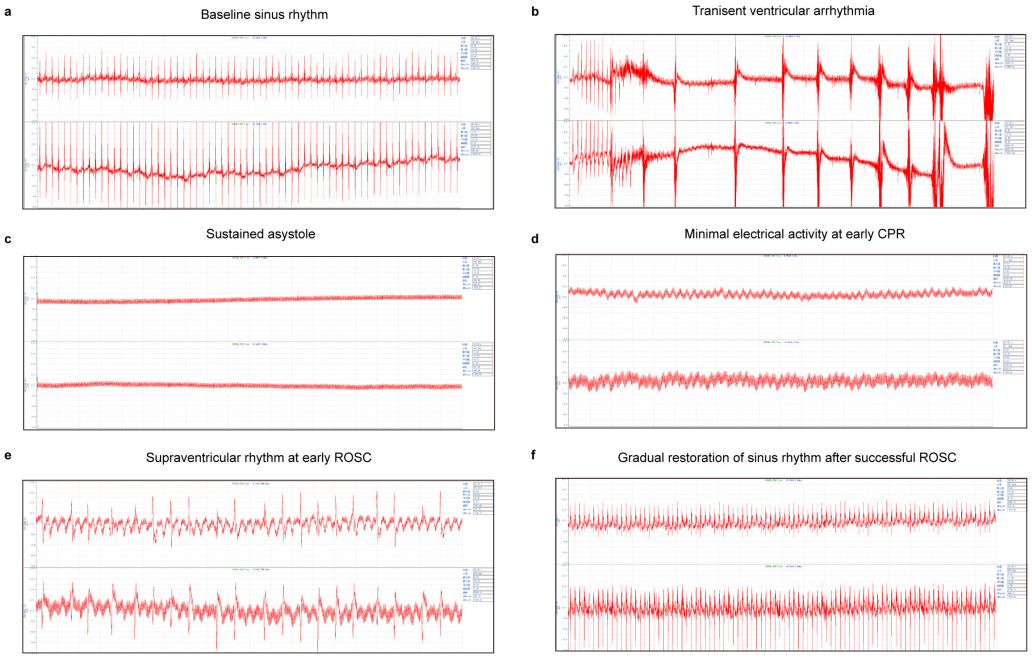

Supplementary Fig. 8 | Electrocardiography (ECG) characteristics of the mouse cardiac arrest and cardiopulmonary resuscitation (CA/CPR) model. Representative ECG traces illustrating the dynamic progression of the CA/CPR model: (**a**) baseline sinus rhythm; (**b**) tranisent ventricular arrhythmia; (**c**) sustained asystole; (**d**) minimal electrical activity at early CPR; (**e**) supraventricular rhythm at early return of spontaneous circulation (ROSC); (**f**) gradual restoration of sinus rhythm after successful ROSC.

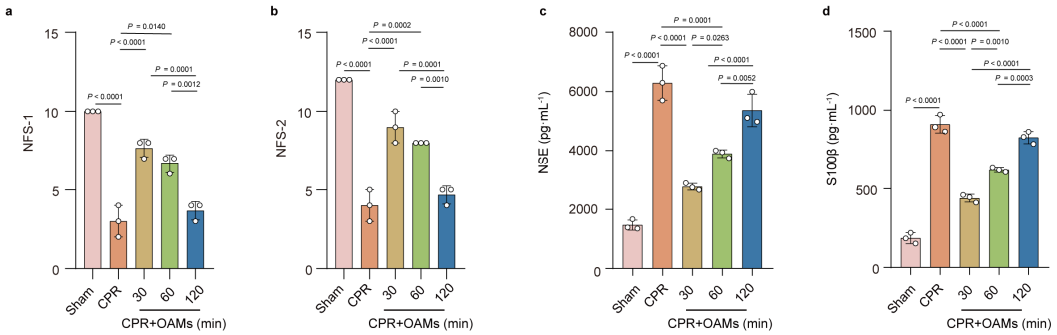

Supplementary Fig. 9 | Efficacy of delayed OAM administration following CA/CPR. a, b, Neurological function scores NFS-1 (**a**) and NFS-2 (**b**) assessed at 24 h after ROSC in mice receiving OAMs at delayed time points of 30, 60, or 120 min post-ROSC. Art-equivalent dose, 5 mg kg^{-1}. *n* = 3 mice. **c, d**, Serum concentrations of neuro-injury biomarkers neuron-specific enolase (NSE; **c**) and S100β (**d**) measured by ELISA at 24 h after ROSC in mice treated with OAMs at the indicated delayed time points. Art-equivalent dose, 5 mg kg^{-1}. *n* = 3 mice. Data are presented as mean ± SD. Statistical significance was determined by one-way ANOVA with Tukey's post hoc test (multiple groups).

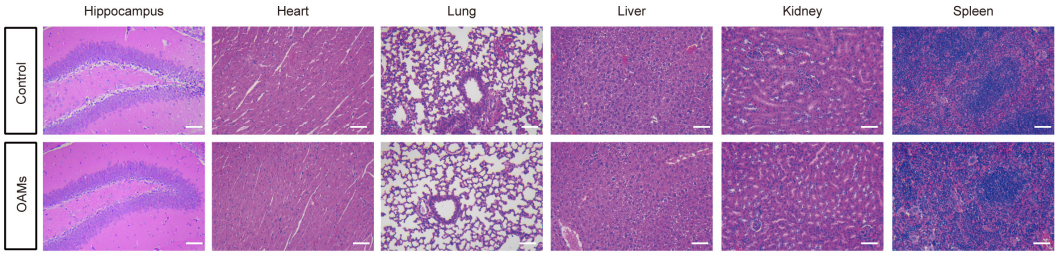

Supplementary Fig. 10 | Histological assessment of major organs following OAM administration. Haematoxylin and eosin (H&E) staining of hippocampus, heart, lung, liver, kidney, and spleen collected 24 h after *i.v.* administration of PBS (control) or OAMs. Art-equivalent dose, 5 mg kg^{-1}. Scale bars, 100 μm. The images are representative of $n = 3$ biological replicates.

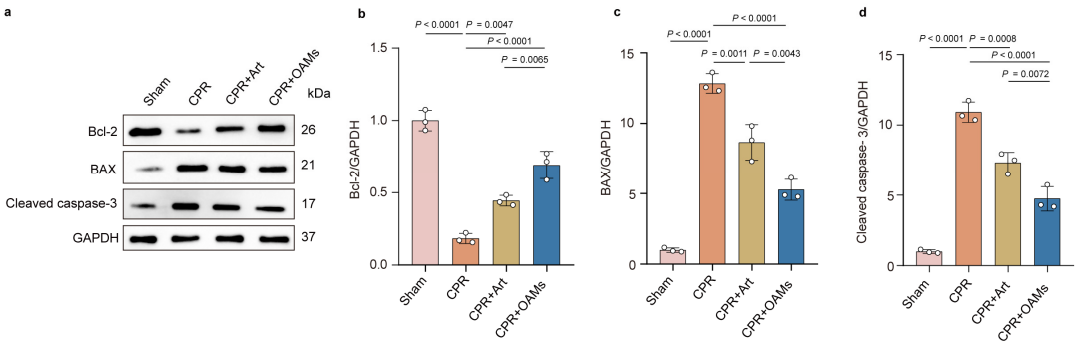

Supplementary Fig. 11 | OAM-mediated regulation of apoptotic pathways after CA/CPR. Western blots (**a**) and quantification of hippocampal expression of Bcl-2 (**b**), BAX (**c**), and cleaved caspase-3 (**d**) at 24 h after ROSC in mice receiving *i.v.* administration of the indicated treatments immediately post-ROSC. Art-equivalent dose, 5 mg kg^{-1}. The blots are representative of $n = 3$ biological replicates. Data are presented as mean ± SD. Statistical significance was determined by one-way ANOVA with Tukey's post hoc test (multiple groups).

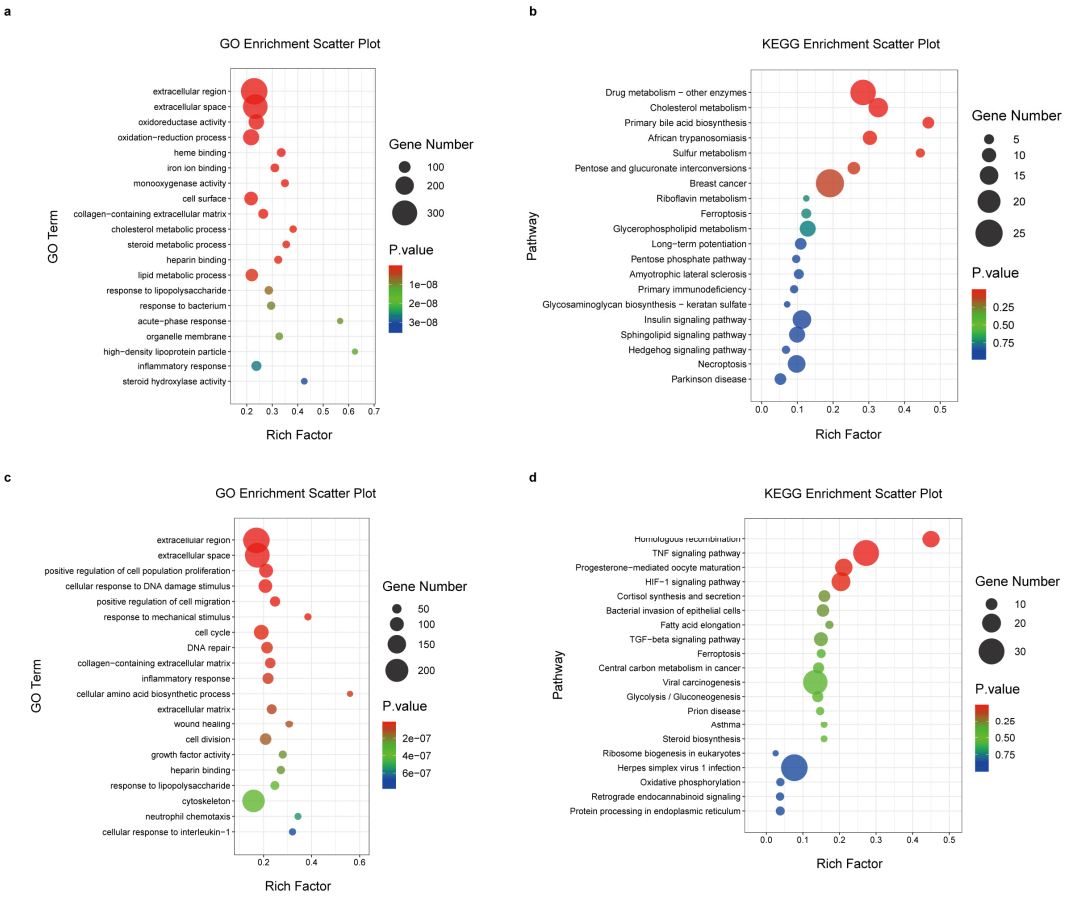

Supplementary Fig. 12 | Functional enrichment analysis of differentially expressed genes (DEGs) under H/R and OAM treatment. a, b, Top 20 enriched Gene Ontology (GO) biological process terms (**a**) and KEGG pathways (**b**) for DEGs between NC and H/R groups (n = 3 biological replicates). **c, d**, Top 20 enriched GO biological process terms (**c**) and KEGG pathways (**d**) for DEGs between H/R and H/R+OAMs groups. Art-equivalent dose, 250 nM. n = 3 biological replicates.

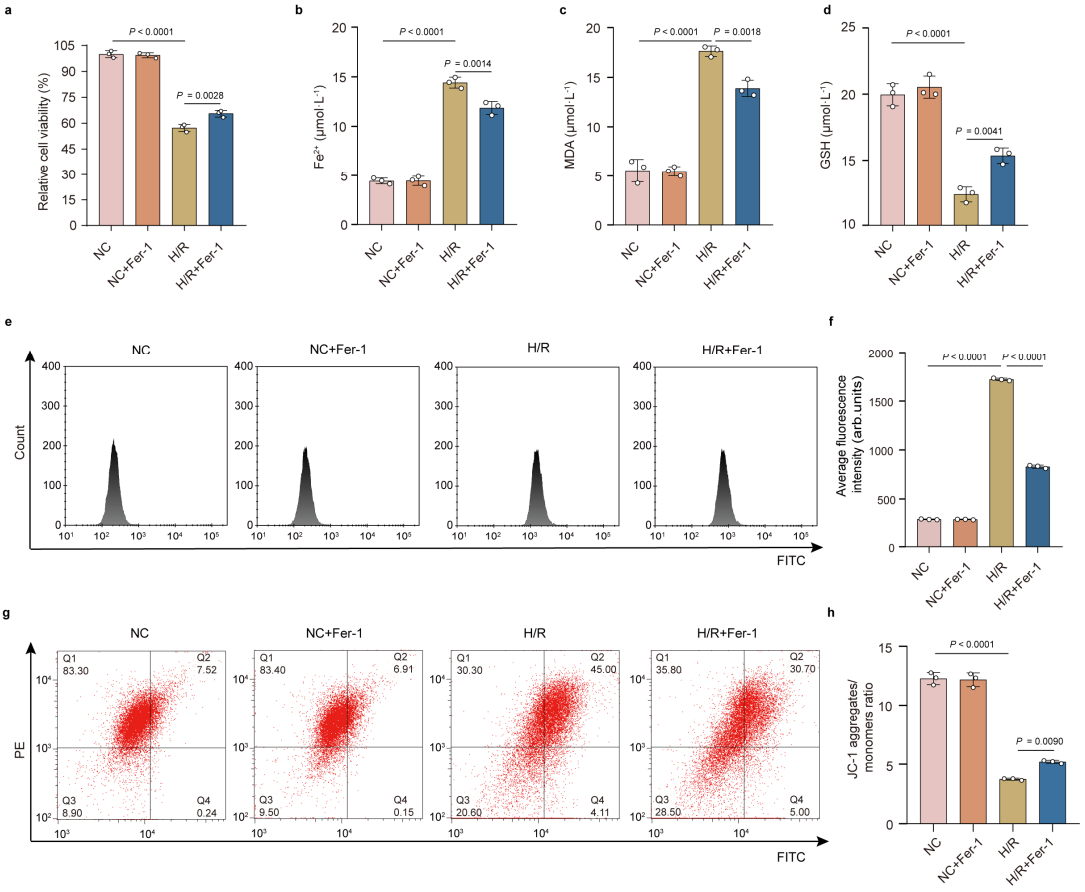

Supplementary Fig. 13 | Ferrostatin-1 (Fer-1) alleviates H/R-induced ferroptosis in HT22 neurons. a, Cell viability after Fer-1 treatment under H/R for 24 h. **b**, Intracellular Fe^{2+} levels measured by the Ferrozine assay. *n* = 3 independent experiments. **c, d**, Levels of malondialdehyde (MDA, c) and glutathione (GSH, d) assessed by thiobarbituric acid (TBA) colourimetry and 5,5'-dithiobis-(2-nitrobenzoic acid) (DTNB) assays, respectively. *n* = 3 independent experiments. **e, f**, Representative flow cytometry histograms (**e**) and quantification (**f**) of cytosolic lipid ROS using C11-BODIPY 581/591 probe. *n* = 3 independent experiments. **g, h**, Representative flow cytometry dot plots (**g**) and quantification (**h**) of mitochondrial membrane potential (ΔΨm) assessed by JC-1 staining. JC-1 forms red-fluorescent aggregates in mitochondria with intact ΔΨm and green-fluorescent monomers upon depolarisation. ΔΨm changes are expressed as the JC-1 aggregate/monomer ratios. *n* = 3 independent experiments. Fer-1 dose, 5 μM. Data are presented as mean ± SD. Statistical significance was determined by one-way ANOVA with Tukey's post hoc test (multiple groups).

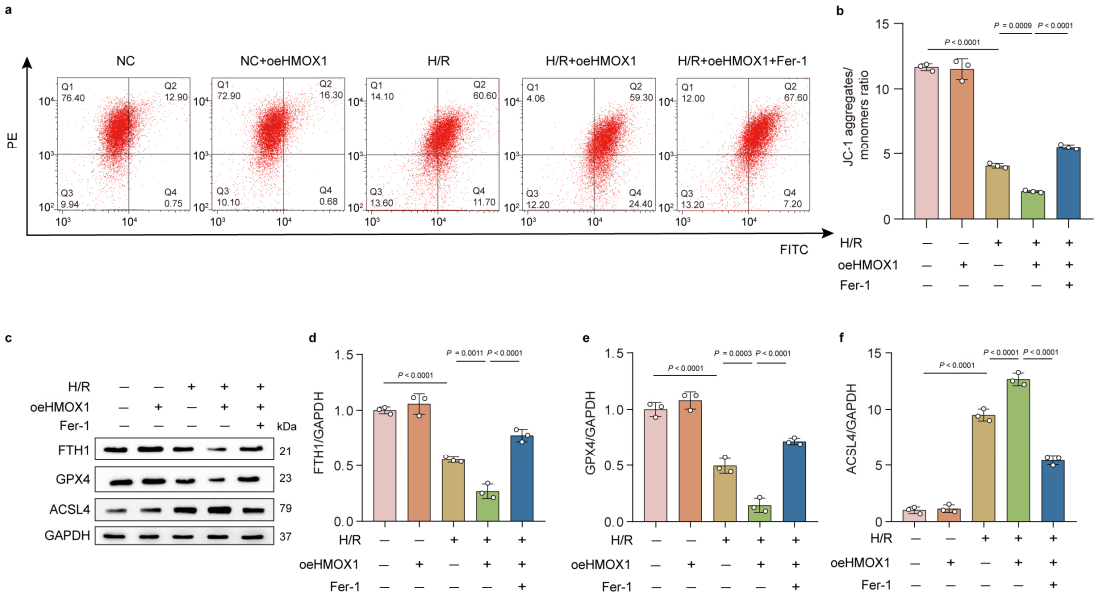

Supplementary Fig. 14 | HMOX1 overexpression exacerbates ferroptotic signalling. a, b, Representative flow cytometry dot plots (**a**) and quantification (**b**) of ΔΨm assessed by JC-1 staining in control and HMOX1-overexpressing (oeHMOX1) HT22 cells treated with Fer-1 under H/R conditions for 24 h. Fer-1 dose, 5 μM. $n = 3$ independent experiments. **c–f**, Western blots (**c**) and quantitative analysis of ferroptosis-related proteins FTH1 (**d**), GPX4 (**e**), and ACSL4 (**f**), with GAPDH as loading control. Fer-1 dose, 5 μM. The blots are representative of $n = 3$ biological replicates. Data are presented as mean ± SD. Statistical significance was determined by one-way ANOVA with Tukey's post hoc test (multiple groups).

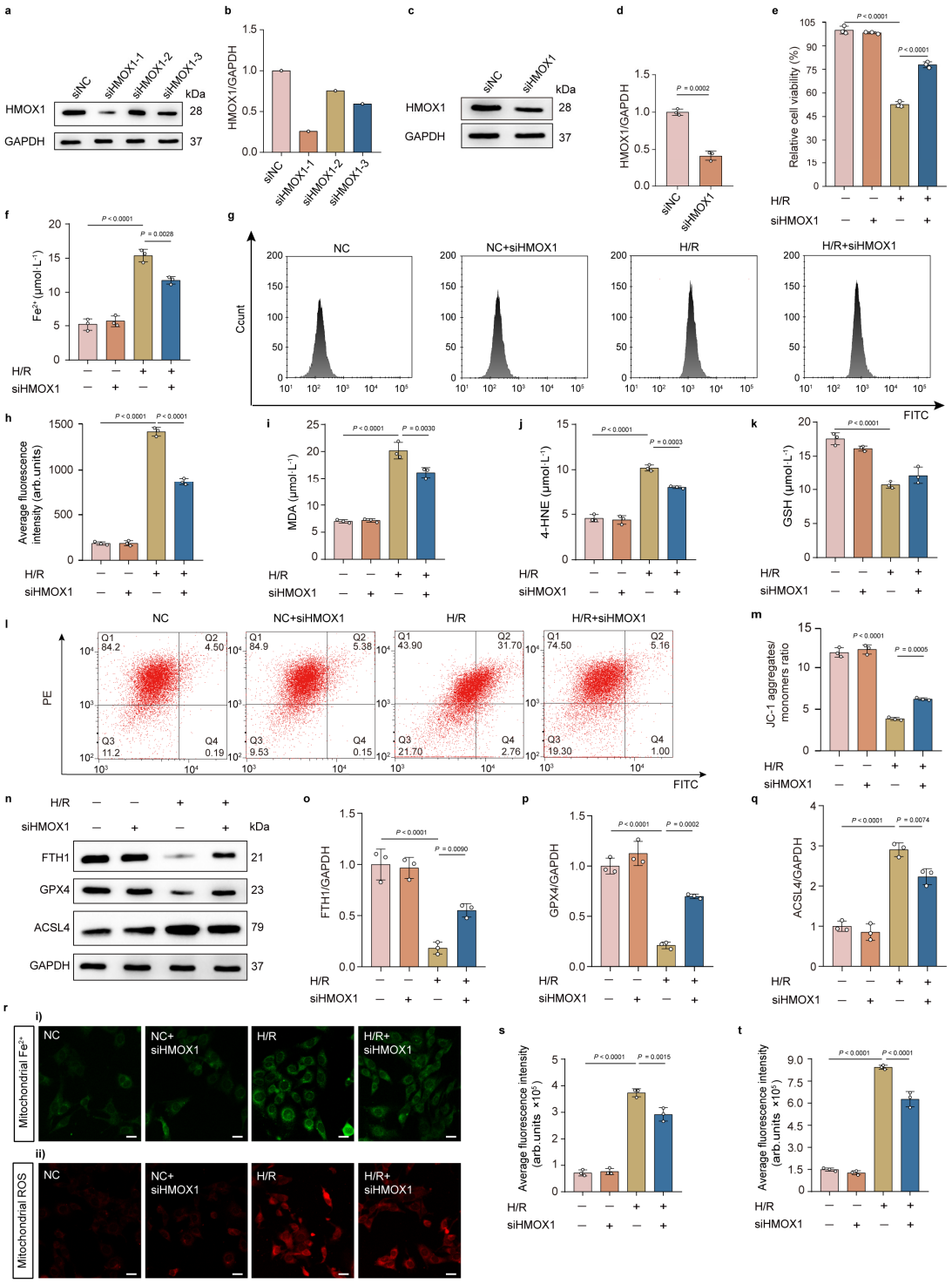

Supplementary Fig. 15 | HMOX1 knockdown alleviates ferroptosis in HT22 neurons under H/R. a, b, Western blots (**a**) and quantification (**b**) of HMOX1 protein levels in HT22 cells transfected with non-targeting control siRNA (siNC) or three HMOX1-targeting siRNAs (siHMOX1-1, siHMOX1-2, siHMOX1-3) under basal conditions. The blots are representative of $n = 3$ biological replicates. **c, d**, Western blots (**c**) and densitometric analysis (**d**) confirming the siHMOX1 knockdown

efficiency. The blots are representative of $n = 3$ biological replicates. **e, f**, Cell viability (e, CCK-8 assay) and cytosolic Fe2+ levels (f, ferrozine assay) in siNC and siHMOX1 HT22 cells after 24 h of H/R. $n = 3$ independent experiments. **g, h**, Representative flow cytometry histograms (**g**) and quantification (**h**) of cytosolic lipid ROS in siNC and siHMOX1 cells under H/R for 24 h, detected using C11-BODIPY 581/591 probe. $n = 3$ independent experiments. **i–k**, Quantification of ferroptosis-related biochemical markers in siNC and siHMOX1 cells after 24 h of H/R: MDA (**i**, TBA method), 4-HNE (**j**, ELISA), and GSH (**k**, DTNB method). $n = 3$ independent experiments. **l, m**, Representative JC-1 flow cytometry dot plots (**l**) and quantification (**m**) of mitochondrial membrane potential in siNC and siHMOX1 cells after 24 h of H/R, expressed as the JC-1 aggregate/monomer ratios. $n = 3$ independent experiments. **n–q**, Western blots (**n**) and relative expression of FTH1 (**o**), GPX4 (**p**), and ACSL4 (**q**) in siNC and siHMOX1 cells under H/R for 24 h, with GAPDH as loading control. The blots are representative of $n = 3$ biological replicates. **r–t**, Confocal images (**r**) of mitochondrial Fe^{2+} (Mito-FerroGreen, green; **r-i**) and mitochondrial lipid ROS (MitoSOX Red, red; **r-ii**) in siNC and siHMOX1 cells after 24 h of H/R, and corresponding quantitative analysis of mitochondrial Fe^{2+} (**s**) and mitochondrial lipid ROS (**t**). Scale bar, 25 μm. The blots are representative of $n = 3$ biological replicates. Data are presented as mean ± SD. Statistical significance was determined by a two-tailed unpaired Student's *t* test (two groups) or one-way ANOVA with Tukey's post hoc test (multiple groups).

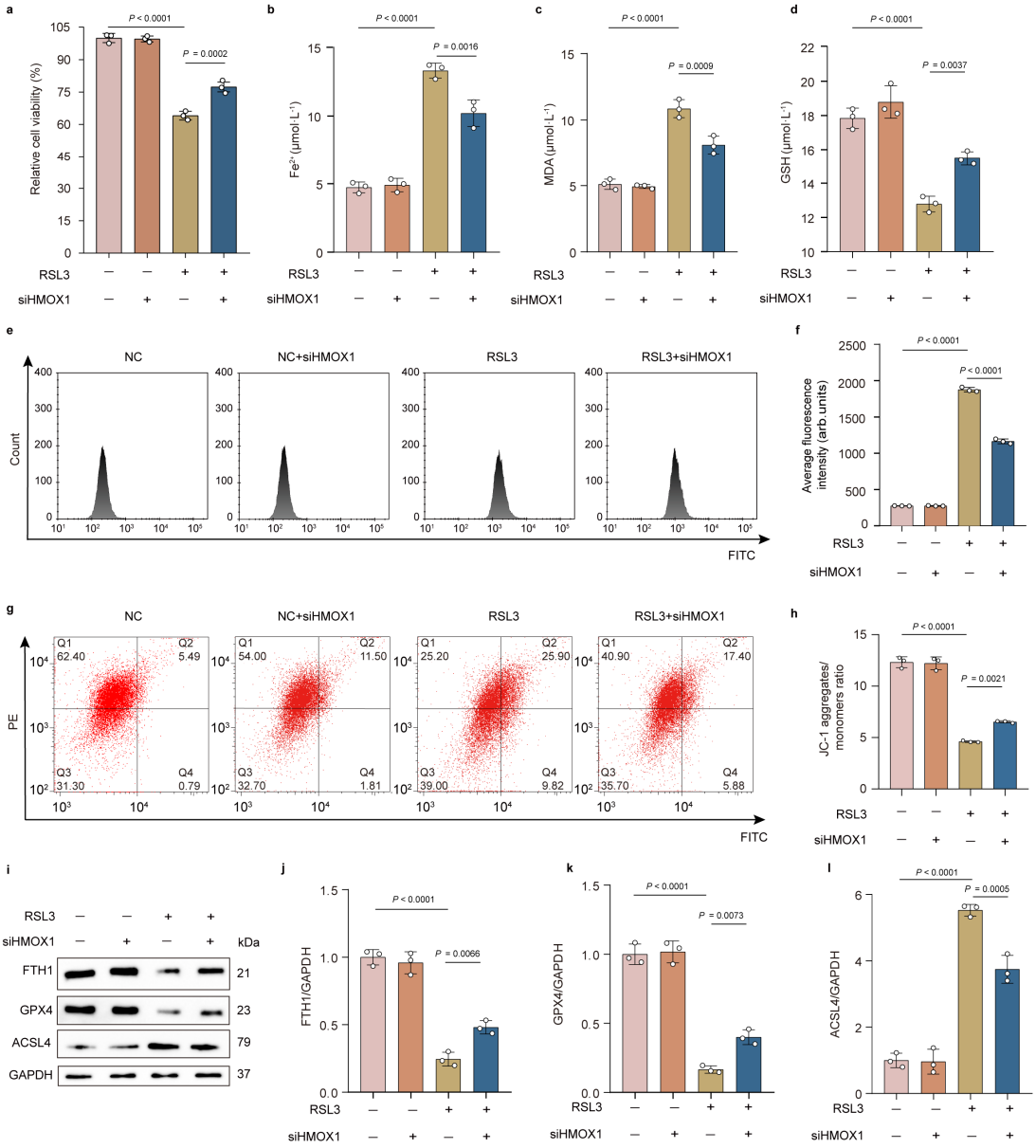

Supplementary Fig. 16 | HMOX1 knockdown attenuates RSL3-induced ferroptosis in HT22 neurons. a–d, Cell viability (**a**, CCK-8 assay), cytosolic Fe^{2+} levels (**b**, ferrozine assay), MDA levels (**c**, TBA method), and GSH content (**d**, DTNB method) in siNC and siHMOX1 HT22 cells treated with RSL3 for 24 h under basal culture conditions. *n* = 3 independent experiments. **e, f**, Representative flow cytometry histograms (**e**) and quantification (**f**) of cytosolic lipid ROS in siNC and siHMOX1 cells following 24 h of RSL3 treatment, detected using C11-BODIPY 581/591. *n* = 3 independent experiments. **g, h**, Representative JC-1 flow cytometry dot plots (**g**) and quantification of mitochondrial membrane potential (**h**) in siNC and siHMOX1 cells after 24 h of RSL3 exposure. *n* = 3 independent experiments. **i–l**, Western blots (**i**) and

relative expression of FTH1 (**j**), GPX4 (**k**), and ACSL4 (**l**) in siNC and siHMOX1 cells treated with RSL3 for 24 h, with GAPDH as loading control. The blots are representative of $n = 3$ biological replicates. RSL3 dose, 150 nM. Data are presented as mean ± SD. Statistical significance was determined by one-way ANOVA with Tukey's post hoc test (multiple groups).

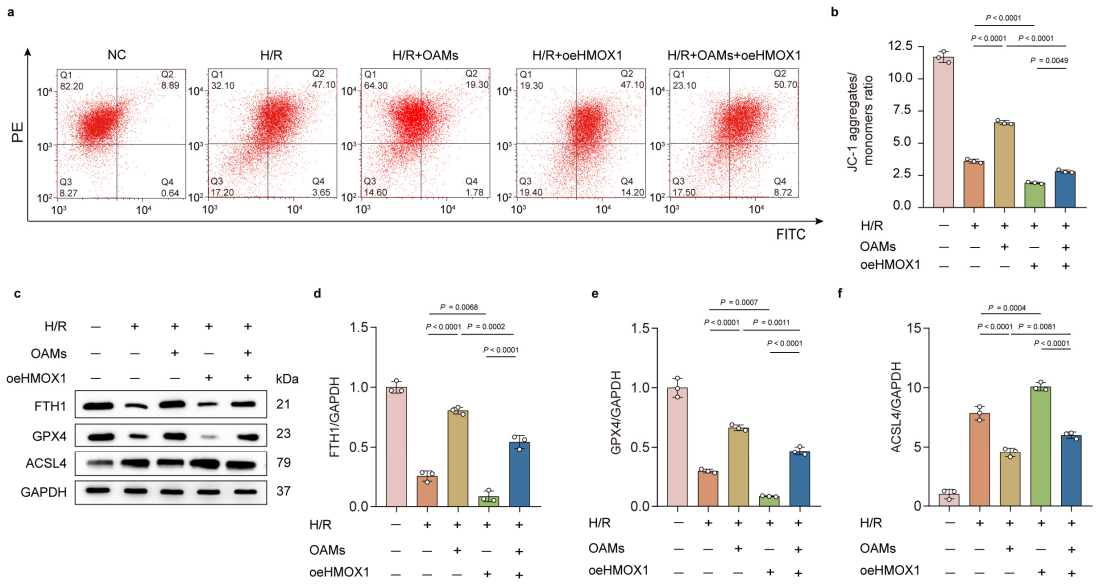

Supplementary Fig. 17 | OAMs attenuate HMOX1-overexpression–induced ferroptosis and mitochondrial dysfunction in HT22 neurons under H/R. a, b, Representative JC-1 flow cytometry dot plots (**a**) and quantification of mitochondrial membrane potential (**b**) in control and oeHMOX1 HT22 cells treated with OAMs under H/R conditions for 24 h. n = 3 independent experiments. **c–f**, Western blots (**c**) and relative expression levels of FTH1 (**d**), GPX4 (**e**), and ACSL4 (**f**) in control and oeHMOX1 HT22 cells treated with OAMs under H/R conditions for 24 h. The blots are representative of n = 3 biological replicates. Art-equivalent dose, 250 nM. Data are presented as mean ± SD. Statistical significance was determined by one-way ANOVA with Tukey's post hoc test (multiple groups).

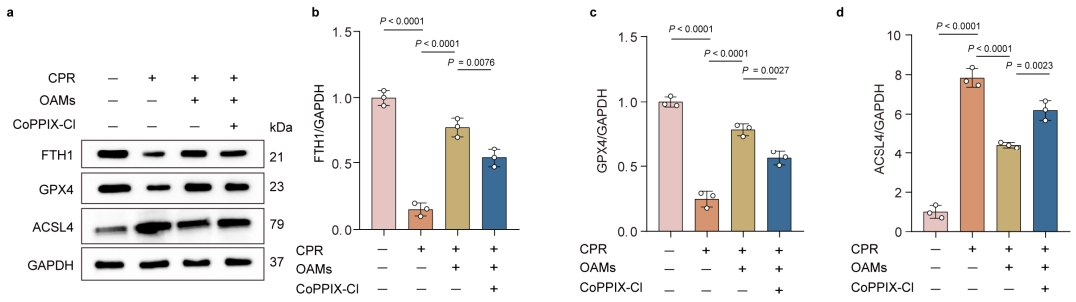

Supplementary Fig. 18 | CoPPIX-Cl–mediated HMOX1 activation weakens OAM-mediated regulation of ferroptosis-related proteins in CA/CPR mice. a–d, For CA/CPR mice receiving OAMs, CoPPIX-Cl, or their combination immediately after ROSC, Western blot bands (**a**) and relative expression of FTH1 (**b**), GPX4 (**c**), and ACSL4 (**d**) in hippocampal tissue at 24 h post-ROSC. Art-equivalent dose, 5 mg kg^{-1}; CoPPIX-Cl–equivalent dose, 10 mg kg^{-1}. The blots are representative of $n = 3$ biological replicates. Data are presented as mean ± SD. Statistical significance was determined by one-way ANOVA with Tukey's post hoc test (multiple groups).

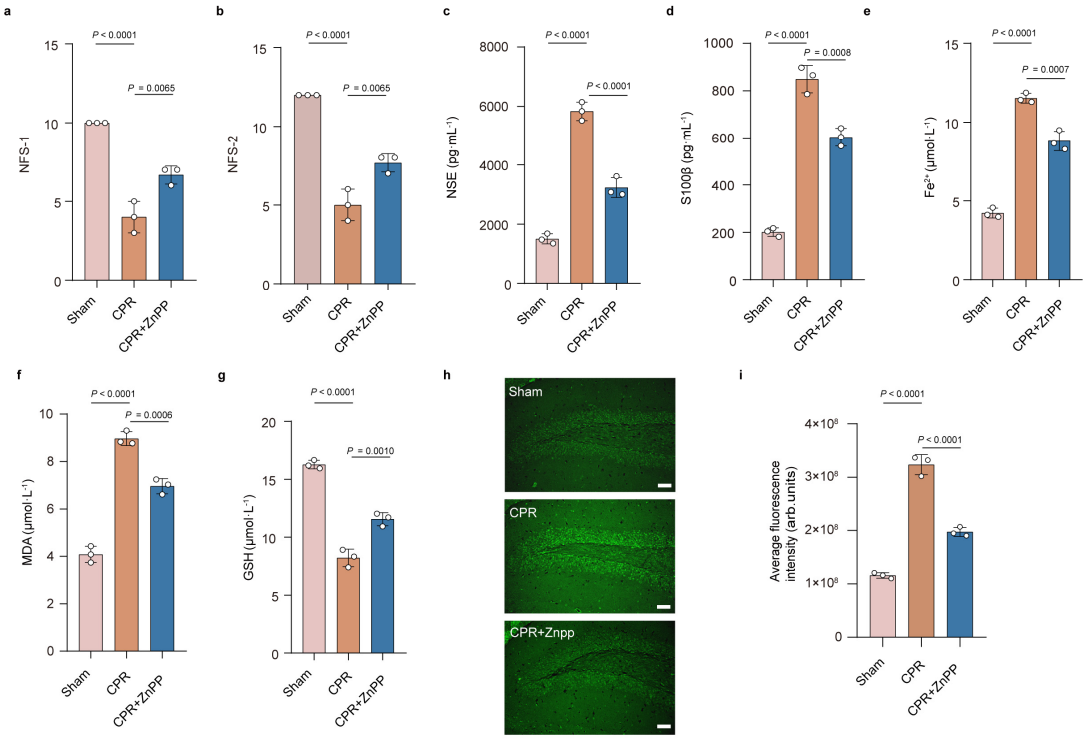

Supplementary Fig. 19 | HMOX1 inhibition alleviates post-resuscitation brain injury by suppressing ferroptosis *in vivo*. a, b, Neurological function scores (NFS-1, **a**; NFS-2, **b**) in CA/CPR mice receiving a single intraperitoneal (*i.p.*) injection of ZnPP 24 h before CA induction, assessed at 24 h post-ROSC. $n = 3$ mice. **c, d**, Serum levels of neuronal injury biomarkers NSE (**c**) and S100β (**d**) measured by ELISA at 24 h post-ROSC. $n = 3$ mice. **e–g**, Quantification of ferroptosis-related biochemical markers in hippocampal tissue from each group: cytosolic Fe^{2+} levels determined by ferrozine assay (**e**), MDA levels by TBA method (**f**), and GSH content by DTNB assay (**g**). $n = 3$ mice. **h, i**, Representative DCFH-DA fluorescence images (**h**) and quantitative analysis (**i**) of ROS levels in the dentate gyrus (DG) region of the hippocampus at 24 h post-ROSC. ROS signals are shown as green fluorescence. Scale bar, 100 μm. The images are representative of $n = 3$ biological replicates. ZnPP-equivalent dose, 10 mg kg^{-1}. Data are presented as mean ± SD. Statistical significance was determined by one-way ANOVA with Tukey's post hoc test (multiple groups).

Supplementary Tables

Supplementary Table 1. Baseline and CPR characteristics of mice in Fig. 5.

Parameters	Sham	CPR	CPR+Art	CPR+OAMs	*P* value
Body weight, g	24.57±0.69	23.83±1.00	23.08±1.00	23.63±0.98	0.078
Heart rate, bpm	437.5±10.15	430.33±62.91	434.5±57.29	441.5±26.28	0.793
Body temperature, ℃	36.62±0.12	36.62±0.16	36.63±0.12	36.6±0.15	0.911
CPR time, min	/	4.00±0.89	5.33±1.21	4.17±1.47	0.172
Epinephrine dosage, μg	/	6.40±1.43	8.53±1.94	6.67±2.36	0.172

Note: "/" indicates that the measurement is not applicable to the Sham group, as no CPR procedure was performed. n = 6 mice. Art-equivalent dose, 5 mg kg^{-1}. Data are presented as mean ± SD. Multi-group comparisons used one-way ANOVA for normally distributed data (Shapiro-Wilk test $P > 0.05$) or Kruskal-Wallis H test for non-normally distributed data (Shapiro-Wilk test $P \leq 0.05$). All statistical tests were two-sided, and $P < 0.05$ was considered statistically significant.

Supplementary Table 2. Baseline and CPR characteristics of mice in Supplementary Fig. 9.

Parameters	Sham	CPR	CPR+OAMs 30 min	CPR+OAMs 60 min	CPR+OAMs 120 min	*P* value
Body weight, g	24.43±0.47	24.13±0.80	24.47±0.50	24.6±0.46	24.3±0.17	0.840
Heart rate, bpm	390.67±2.08	392.00±35.55	379.33±5.03	407.33±23.16	403.33±11.727	0.479
Body temperature, ℃	36.6±0.10	36.67±0.15	35.6±1.56	36.63±0.12	36.6±0.35	0.363
CPR time, min	/	4.58±1.51	3.78±1.02	3.92±0.88	4.89±1.17	0.621
Epinephrine dosage, μg	/	8.00±1.60	6.40±1.60	6.40±1.60	8.00±1.60	0.441

Note: "/" indicates that the measurement is not applicable to the Sham group, as no CPR procedure was performed. n = 3 mice. Art-equivalent dose, 5 mg kg^{-1}. Data are presented as mean ± SD. Multi-group comparisons used one-way ANOVA or Kruskal-Wallis H test. All statistical tests were two-sided, and $P < 0.05$ was considered statistically significant.

Supplementary Table 3. Blood routine parameters of C57BL/6 mice at 24 h after treatments.

Parameters	Control	OAMs	*P* value
WBC, $\times 10^9$ L^{-1}	5.82±0.25	5.84±0.43	0.930
NEU, %	18.10±1.35	17.80±1.46	0.745
LY, %	64.18±6.28	66.67±2.94	0.447
RBC, $\times 10^{12}$ L^{-1}	6.55±0.26	6.34±0.08	0.117
HGB, g L^{-1}	208.66±4.55	204.60±2.05	0.106
HCT, %	34.88±1.49	33.96±0.34	0.215
PLT, $\times 10^9$ L^{-1}	308.80±35.57	319.40±37.41	0.658

Venous blood was collected at 24 h after administration from PBS (Control) and OAMs-treated mice for analysis. $n = 5$ mice. Art-equivalent dose, 5 mg kg^{-1}. Data are presented as mean ± SD. Differences between the two groups were analysed using two-tailed unpaired Student's *t* test for normally distributed data or Mann-Whitney U test for non-normally distributed data. All statistical tests were two-sided, and $P < 0.05$ was considered statistically significant. WBC, white blood cells; NEU, neutrophils; LY, lymphocytes; RBC, red blood cells; HGB, haemoglobin; HCT, haematocrit; PLT, platelets.

Supplementary Table 4. Biochemical parameters of C57BL/6 mice at 24 h after treatments.

Parameters	Control	OAMs	*P* value
NSE, ng ml^{-1}	1.49±0.33	1.68±0.36	0.420
cTN-I, pg ml^{-1}	23.48±3.02	26.17±3.25	0.213
SP-D, pg ml^{-1}	2.88±0.73	3.22±0.62	0.453
ALT, U l^{-1}	23.06±3.6	22.31±4.17	0.771
Cr, μmol l^{-1}	51.94±4.49	52.82±2.43	0.709

Plasma was collected at 24 h after administration from PBS (Control) and OAMs-treated mice for analysis. $n = 5$ mice. Art-equivalent dose, 5 mg kg^{-1}. Data are presented as mean ± SD. Differences between the two groups were analysed using two-tailed unpaired Student's *t* test or Mann-Whitney U test. All statistical tests were two-sided, and $P < 0.05$ was considered statistically significant. NSE (neuron-specific enolase) for brain injury; cTN-I (cardiac troponin I) for myocardial injury; SP-D (surfactant protein D) for lung injury; ALT (alanine aminotransferase) for hepatic injury; and Cr (creatinine) for renal injury.

Supplementary Table 5. Baseline and CPR characteristics of mice in Fig. 10.

Parameters	Sham	CPR	CPR+OAMs	CPR+OAMs+ CoPPIX-Cl	*P* value
Body weight, g	21.59±0.77	21.33±1.01	20.96±0.83	21.23±0.91	0.501
Heart rate, bpm	374.75±24.26	372.75±17.81	369.25±21.79	376.88±17.72	0.913
Body temperature, ℃	36.64±0.17	36.73±0.11	36.61±0.14	36.64±0.17	0.301
CPR time, min	/	3.56±0.73	3.69±0.86	3.88±1.02	0.801
Epinephrine dosage, μg	/	6.00±1.06	6.00±1.06	6.40±1.39	0.806

Note: "/" indicates that the measurement is not applicable to the Sham group, as no CPR procedure was performed. $n = 8$ mice. Art-equivalent dose, 5 mg kg^{-1}; CoPPIX-Cl-equivalent dose, 10 mg kg^{-1}. Data are presented as mean ± SD. Multi-group comparisons used one-way ANOVA or Kruskal-Wallis H test. All statistical tests were two-sided, and $P < 0.05$ was considered statistically significant.

Supplementary Table 6. Baseline and CPR characteristics of mice in Supplementary Fig. 18.

Parameters	Sham	CPR	CPR+ZnPP	*P* value
Body weight, g	24.47±0.38	24.17±0.25	24.00±0.78	0.581
Heart rate, bpm	386.67±7.64	391.00±26.89	414.00±22.52	0.295
Body temperature, ℃	36.50±0.00	36.53±0.06	36.63±0.12	0.154
CPR time, min	/	4.09±1.60	4.78±1.02	0.565
Epinephrine dosage, μg	/	6.93±2.44	8.53±0.92	0.349

Note: "/" indicates that the measurement is not applicable to the Sham group, as no CPR procedure was performed. $n = 3$ mice. ZnPP-equivalent dose, 10 mg kg^{-1}. Data are presented as mean ± SD. Differences between the two groups were analyzed using a two-tailed unpaired Student's *t* test or Mann-Whitney U test, and multi-group comparisons used one-way ANOVA or Kruskal-Wallis H test. All statistical tests were two-sided, and $P < 0.05$ was considered statistically significant.

Supplementary Table 7. qPCR primer sequences

Gene	Forward primer	Reverse primer
Tnf-α	CCCTCACACTCAGATCATCTTCT	GCTACGACGTGGGCTACAG
Il-1β	GAAATGCCACCTTTTGACAGTG	TGGATGCTCTCATCAGGACAG
Egr1	AGTGATGAACGCAAGAGGCA	GGGAGAAAAGGTCGCTGTCA
Timp1	AGACCACCTTATACCAGCGT	AGGACCTGATCCGTCCACAA
Il6	TAGTCCTTCCTACCCCAATTTCC	TTGGTCCTTAGCCACTCCTTC
Hmox1	CCTCACAGATGGCGTCACTT	TGGGGGCCAGTATTGCATTT
Ahcy	ACAAGCCCAGGTCACAAACA	AAGCGATGGGACATCTGGTG
Kif20a	CAGCGGGCTTACTCTCTGATG	GTCTGACAACAGGTCCTTTCG
Gja1	AAAGGCGTGAGGGAAGTACC	ACAGCGAAAGGCAGACTGTT
Pdss2	AGCAGATTGGAGAGGCTCAA	TAAAGCCGATCTGGCCTCTGA
Gapdh	GACAGCCGCATCTTCTTGTG	AATCCGTTCACACCGACCTT

Supplementary Table 8. Antibody information

Antibody name	Lot number	Clone name	Catalog number	Dilutions	Company
GAPDH	#10	14C10	#2118	1:5000	CST
Iba1	#3	E4O4W	#17198	1:1000	CST
CD31	#YZUO122052	Polyclonal	#AF3628	1:200	R&D systems
NeuN	#23	D4G4O	#24307	1:1000	CST
HMOX1	#14	E3F4S	#43966	1:1000	CST
β-actin	#7	13E5	#4970	1:1000	CST
NCOA4	/	EPR28511-12	#ab314553	1:1000	Abcam
NCOA4	/	H00008031-M04	#H00008031-M04	1:1000	Thermofisher
FTH1	#N19MA05	Polyclonal	#R23306	1:1000	Zenbio
LC3	#00119545	Polyclonal	#14600-1-AP	1:1000	Proteintech
GPX4	#10026631	3F5G5	#67763-1-IG	1:1000	Proteintech
ACSL4	#10018706	Polyclonal	#22401-1-AP	1:1000	Proteintech
iNOS	#GR3248775-14	EPR16635	#ab178945	1:200	Abcam
Arg1	#00069077	Polyclonal	#16001-1-AP	1:200	Proteintech
BAX	#N02JL09	Polyclonal	#R22708	1:1000	Zenbio
Bcl-2	#N01JL01	Polyclonal	#381702	1:1000	Zenbio
Cleaved caspase-3	#7	ASP175	#9661S	1:500	CST

Supplementary Table 9. Knockdown primer sequences

siRNA	Sense	Anti-sense
Control-siRNA	AUGAGAUAAGCUUAAGAUCGC	GCGAUCUUAAGCUUAUCUCAU
Hmox1-siRNA1	ACAGUGGCAGUGGGAAUUUAU	AUAAAUUCCCACUGCCACUGU
Hmox1-siRNA2	AGCCACACAGCACUAUGUAAA	UUUACAUAGUGCUGUGUGGCU
Hmox1-siRNA3	GAUGGCUUCCUUGUACCAUAU	AUAUGGUACAAGGAAGCCAUC
Ncoa4-siRNA1	GCAAAUUAAAGAUAAUUUACG	UAAAUUAUCUUUAAUUUGCUG
Ncoa4-siRNA2	GGAGUAUACUCAGAACAAAGA	UUUGUUCUGAGUAUACUCCAG
Ncoa4-siRNA3	CAAUUGUCUUAUUCAUCAACU	UUGAUGAAUAAGACAAUUGAA